Synthesis and Dynamic Stereochemistry of Tris(2-methyl-1-azulenyl)methyl Cation and the Corresponding Methane Derivative. Evidence That the Conjugative Effect Largely Contributes to the Transition State of the Ring Flipping[1)]

Shunji Ito, Noboru Morita, and Toyonobu Asao*

Department of Chemistry, Faculty of Science, Tohoku University, Kawauchi, Aoba-ku, Sendai 980-77

(Received March 2, 1995)

The stable carbocation, tris(2-methyl-1-azulenyl)methyl hexafluorophosphate (**4**·PF_6^-) was prepared by a hydride-abstraction reaction of the corresponding methane derivative, tris(2-methyl-1-azulenyl)methane (**5**). The dynamic stereochemistry of **4** and **5** was studied based on the temperature-dependent ^{1}H NMR spectra, which were analyzed by a flip mechanism; the steric effect of the three 2-methyl groups was also investigated by comparing it with that of the 3,3′,3″-trimethyl analogue, tris(3-methyl-1-azulenyl)methyl hexafluorophosphate (**1b**·PF_6^-). The threshold rotation mechanism for **4** was a two-ring flip, in contrast to a one-ring flip for **1b**, and the activation energies for **4** (78.0 and 73.4 kJ mol^{-1}) were higher than those for **1b** due to increased crowding in the transition state for the rotation. Although the activation energies for **5** (49.9 and 43.2 kJ mol^{-1}) were lower than those for **1b**, the mechanism for **5** was also a two-ring flip. The mechanism was variable between one- and two-ring flip processes due to a steric effect of the three 2-methyl groups. These results indicate that a conjugative interaction between the central cation and the three azulene rings largely contribute to the transition state of the ring flipping as well as to the ground state.

The correlated rotation of a molecular propeller is commonly analyzed in terms of the flip mechanism postulated by Kurkland et al.[2—4)] For a conformational change of this system, the lowest-energy (threshold) rotation mechanism was uniformly a two-ring flip; the mechanism was independent of the conjugative effect between the central atom and the three rings, even in the triphenylmethyl cations[5—7)] and triarylboranes.[8,9)] We have recently reported that the azulene analogues of the triphenylmethyl cation, i.e., tri(1-azulenyl)methyl hexafluorophosphate (**1a**·PF_6^-) and its 3,3′,3″-trimethyl (**1b**·PF_6^-), 3,3′,3″-tris(methoxycarbonyl) (**1c**·PF_6^-), and *t*-butyl (**1d**—**f**·PF_6^-) derivatives, were synthesized by hydride-abstraction reactions of the corresponding hydrocarbons (**2a**—**f**) (Chart 1).[10—12)] These cations (**1a**—**f**) showed extreme stabilities with extraordinary high pK_{R+} values (10.3—14.3).[10—12)] The high stabilities of **1a**—**f** are rationalized by the large conjugative effect between the cationic carbon and the three azulene rings (e.g. **1′**). An analysis of the variable-temperature ^{1}H NMR spectra of the 3,3′,3″-trimethyl derivative (**1b**) indicated that the dynamic stereochemistry of these cations was established in a one-ring flip as the threshold rotation mechanism, which is the first example of a one-ring flip mechanism for a molecular propeller.[12,13)] The one-ring flip mechanism was further supported by a synthesis and analysis of the dynamic stereochemistry of the tri(1-azulenyl)methyl cation containing a different substituent on each azulene ring, i.e., 3-*t*-butyl-3′-methoxycarbonyl-3″-methyltri(1-azulenyl)-methyl hexafluorophosphate (**3**·PF_6^-).[14)]

The one-ring flip is attributable to the large conjugative effect between the cationic carbon and the three azulene rings, so that the large steric interaction among the three rings is expected to shift the threshold rotation mechanism of the tri(1-azulenyl)methyl cation (**1a**) to a two-ring flip. Here, we report that the stable 2,2′,2″-trimethyl derivative, tris(2-methyl-1-azulenyl)methyl hexafluorophosphate (**4**·PF_6^-), and the corresponding methane derivative (**5**) were synthesized in order to increase the steric interaction among the three azulene rings (Chart 2); also, their dynamic stereochemistries were studied using the temperature-dependent ^{1}H NMR spectra based on the flip mechanism.

Results and Discussion

Synthesis. A large steric effect was observed in the synthesis of tris(2-methyl-1-azulenyl)methane (**5**), the precursor for **4**·PF_6^-. The reaction of 2-methylazulene (**6**) with 1-formyl-2-methylazulene (**7**) in acetic acid at room temperature for 21 d, which was under similar conditions to those for the formation of tris(3-methyl-1-

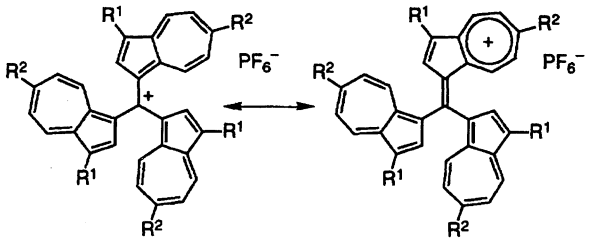

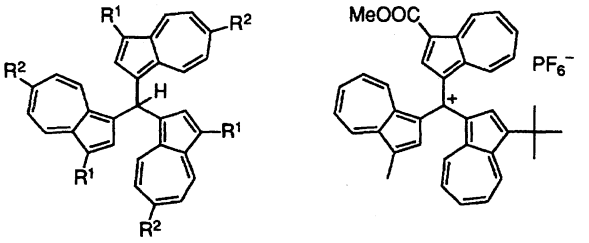

Chart 1.

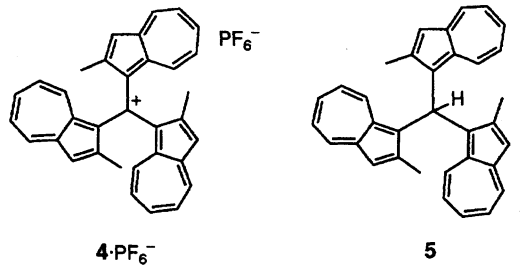

Chart 2.

azulenyl)methane (**2b**),[10,12] the precursor for **1b**·PF_6^-, afforded only a trace amount of **5**, because of the large steric hindrance of the 2-methyl group on the azulene ring for the formation of **5** (Scheme 1). However, the high-pressure reaction (10 kbar) of **6** with **7** in a 50% acetic acid solution of dichloromethane at 30 °C for 1 d, afforded **5** and 1,3-bis[bis(2-methyl-1-azulenyl)methyl]-2-methylazulene (**8**) in 49 and 5% yields, respectively. The hydride abstraction of **5** with DDQ in dichloromethane was proceeded by similar conditions for the formation of **1b**.[10,12] The addition of a 60% aqueous HPF_6 solution to the reaction mixture yielded stable **4**·PF_6^- in quantitative yield.

pK_{R+} Value and the Redox Potentials of 4. The pK_{R+} value and the redox potentials of **4** are summarized in Table 1 along with those of **1b**.[10,12] The pK_{R+} value of **4** (13.4) was determined spectrophotometrically at 24 °C in a buffer solution prepared in 50% aqueous MeCN.[12] The higher pK_{R+} value of **4** compared to that of **1b** (11.4)[10,12] is attributed to an increase in crowding by the three 2-methyl groups, which destabilizes the corresponding hydroxy derivative (Table 1). However, we could not determined the neutralized product of **4** because of the instability of the product. About 70% of the absorption maxima in the visible region of the cation (**4**) was regenerated by immediate acidifying of the alkaline solution of **4** with HCl. The redox potentials (V vs. Ag/Ag^+) of **4**, measured by cyclic voltammetry in MeCN, are also summarized in Table 1, together with those of **1b**.[12] The oxidation of **4** also showed two waves with a narrow interval, i.e., +1.06 and +1.19 V, similar to **1b**, which are due to the oxidation of two azulene rings to give a trication diradical.[12] The first reduction potential of **4** (−0.75 V) was slightly more positive than that of **1b** (−0.82 V), in contrast to the larger pK_{R+} value of **4**.

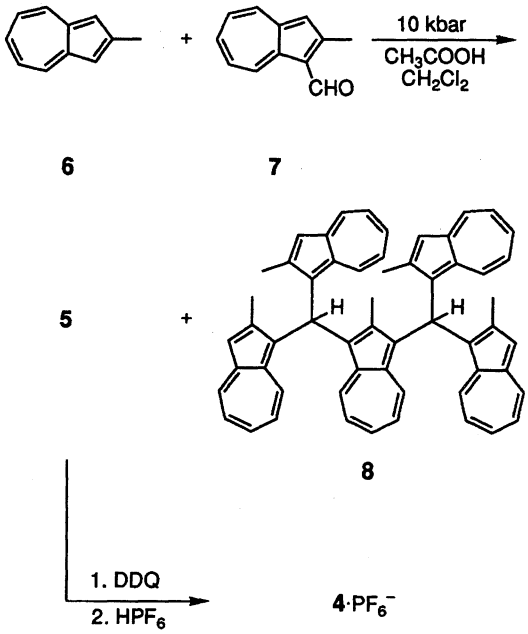

Scheme 1.

Table 1. The pK_{R+} Values[a] and the Redox Potentials[b] of **4** and **1b**[10,12]

	pK_{R+}	E_1^{red}	E_2^{red}	E_1^{ox}	E_2^{ox}
4	13.4±0.1	−0.75	(−1.65)	(+1.06)	(+1.19)
1b	11.4±0.1	−0.82	(−1.59)	(+0.85)	(+0.94)

a) The pK_{R+} values were measured in a buffer solution in 50% aqueous MeCN. b) V. vs. Ag/Ag^+, 0.1 M Et_4NCO_4 in MeCN, Pt electrode, scan rate 100 mV s^{-1}. Irreversible processes were shown in the parentheses.

Dynamic Stereochemistry of the Cation (4). The static ^1H and ^{13}CNMR spectra of **4** and the time-averaged ^1H and ^{13}CNMR spectra of the methane derivative (**5**) at 27 °C are summarized in Tables 2 and 3, respectively. The NMR showed that the rotation

Table 2. ^{1}H NMR Chemical Shifts (ppm) of the Cation (**4**) and the Corresponding Methane Derivative (**5**) at 27 °C

	Solvent	Type[a)]	Assignment							
			CH	2-Me	3	4	5	6	7	8
5	50%CD_2Cl_2/CS_2		7.43	1.79	7.08	8.08	6.99	7.31	6.68	7.60
4	DMSO-d_6	B_3		2.05(a)	7.75	8.68	7.77	7.82	7.27	7.40
		B_2		1.98(b)	7.68	8.69	7.80	7.87	7.34	7.56
		B_1		1.69(c)	7.67	8.71	7.83	7.93	7.43	7.64
		A		1.63(d)	7.61	8.72	7.87	7.99	7.51	7.80

a) A indicates the chemical shifts of the symmetrical stereoisomer of **4** and B_{1-3} show the chemical shifts of the unsymmetrical stereoisomer of **4**.

Table 3. ^{13}C NMR Chemical Shifts (ppm) of the Cation (**4**) and the Corresponding Methane Derivative (**5**) at 27 °C

	Solvent	Type[a)]	Assignment											
			CH or C^+	1	2	2-Me	3	3a	4	5	6	7	8	8a
5	50%CD_2Cl_2/CS_2		37.32	129.31	150.65	16.13	119.55	140.22	134.25	123.00	135.77	122.39	132.26	136.72
4	DMSO-d_6	B_3	154.93	132.86	154.55	15.52	126.55	149.89	138.42	132.61	141.02	132.40	136.08	146.24
		B_2		132.49	154.04	15.21	125.32	148.84	138.82	133.44	141.52	133.08	136.62	145.60
		B_1		133.58	154.53	15.82	127.37	148.17	138.15	131.91	140.69	131.96	135.26	147.00
		A	154.58	133.35	154.04	15.52	126.28	149.24	138.57	132.85	141.24	132.76	135.85	146.37

a) A indicates the chemical shifts of the symmetrical stereoisomer of **4** and B_{1-3} show the chemical shifts of the unsymmetrical stereoisomer of **4**.

of the three azulene rings of **4** was slow on the NMR time scale at that temperature.

The ^{1}H NMR (90 MHz, methyl region) spectra of **4** in DMSO-d_6 at various temperature are shown in Fig. 1. At 30 °C, the NMR spectrum consists of four methyl signals (as indicated a, b, c, and d) in the ratio of ca. 1 : 1 : 1 : 1.5. When the sample was warmed to ca. 80 °C, noticeable line broadening occurred, and further warming resulted in the coalescence of all four peaks to a singlet, which became almost sharp at 120 °C. The possibilities for the isomerization of **4** should be analyzed in terms of the flip mechanism.[2-4)]

Four isomeric propeller conformations (A, $\overline{A}$, B, and $\overline{B}$) are possible for a molecule of this type, as indicated in Fig. 2. $A\overline{A}$ has C_3 symmetry (symmetrical propellers), and each enantiomer has three equivalent methyl groups. $B\overline{B}$ has C_1 symmetry (unsymmetrical propellers), and each enantiomer has three nonequivalent methyl groups. Therefore, the three lower-field resonances (a, b, and c) correspond to those of $B\overline{B}$, while the more intense peak (d) is assigned to those of $A\overline{A}$. The methyl groups of $B\overline{B}$ are tentatively labeled by letters a—c, for convenience, as shown in Fig. 2. The possibilities of interconversions for the stereoisomers of **4** are compatible with those for **1b**.[12,13)] The zero-ring flip processes of **4** ($A \rightarrow \overline{A}$ and $B \rightarrow \overline{B}$) are not detectable by the temperature-dependent ^{1}H NMR spectra, because no methyl group showed a site exchange in this mechanism.[12)] While the three-ring flip process connecting A and $\overline{A}$ also do not show a site exchange, the process connecting B and $\overline{B}$ renders the two azulenyl groups enantiotopic, which shows the site exchange of a

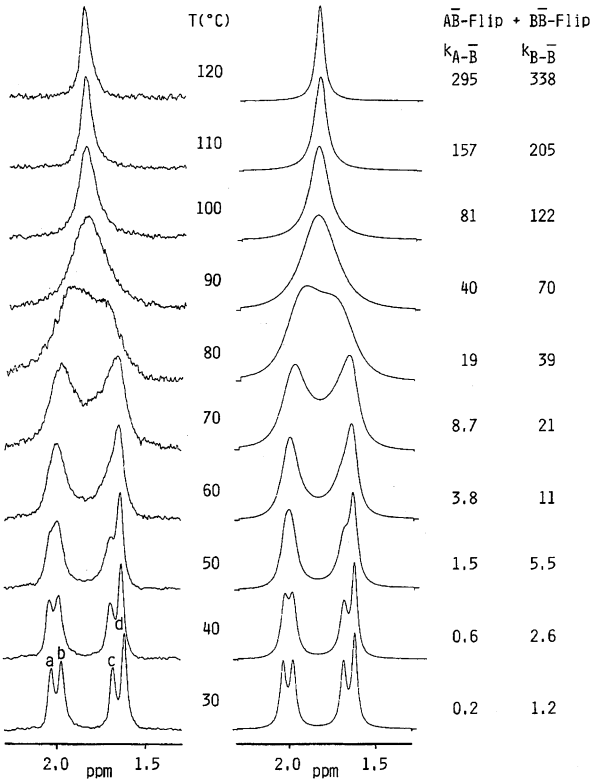

Fig. 1. ^{1}HNMR of **4** (90 MHz, methyl region) in DMSO-d_6 at various temperatures. The left-hand panel displays the experimental spectra. The right-hand panel shows the calculated spectra for the combination of $A \rightarrow \overline{B}$ (or $\overline{A} \rightarrow B$) and $B \rightarrow \overline{B}$ flip.

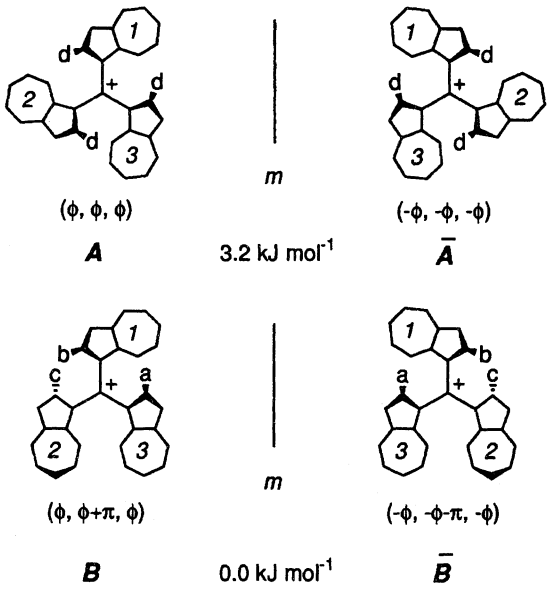

Fig. 2. Stereoisomers of **4**, which were characterized by the torsion angles, and the calculated (PM3) relative heat of formation for those of **4**. Letters a—d are tentatively attached to the methyl groups, corresponding the low-temperature NMR spectrum.

and b. However, the temperature-dependent ^{1}H NMR spectra are unexplainable by the three-ring flip process ($B \rightarrow \overline{B}$). Furthermore, the transition states of the zero- (all three azulene rings rotate through the reference plane) and the three-ring flip processes (all three rings rotate through planes perpendicular to the reference plane) are unfavorable on steric grounds.[12,13] Therefore, they are excluded from an analysis of the dynamic behavior of **4**. The residual one- and two-ring flip mechanisms and the idealized transition states of the two mechanisms for the stereoisomerization of **4** are illustrated in Fig. 3. There is a total of five distinct pathways in the two flip mechanisms (three in the one-ring flip and two in the two-ring flip).

In the one-ring flip (Fig. 3a), the anti-parallel arrangement of the nonflipping two azulene rings (transition state of $A \rightarrow \overline{B}$ (and $\overline{A} \rightarrow B$)) is considered to reduce the steric interaction, compared with the two parallel arrangements (transition states of $B \rightarrow \overline{B}$), because the two transition states of the interconversion of $B \rightarrow \overline{B}$ entail a placement of the 7- and 8-positions and the 2-methyl groups of the nonflipping two azulene rings in essentially the same location, respectively (Fig. 3b). Therefore, the three exchanges (a→d, b→d, and c→d) of the methyl groups by $A \rightarrow \overline{B}$ (and $\overline{A} \rightarrow B$) should be observed as the preferred interconversion in the one-ring flip mechanism.[12]

In the two-ring flip (Fig. 3c), the anti-parallel arrangement of the flipping two azulene rings (transition state of $B \rightarrow \overline{B}$) is considered to reduce the steric interaction, compared with the parallel arrangement (that of $A \rightarrow \overline{B}$), because the transition state of the interconversion of $A \rightarrow \overline{B}$ entails the placement of 8-positions of the flipping two azulene rings in essentially the same location (Fig. 3d). Therefore, the three exchanges (a→b, a→c, and b→c) of the methyl groups by $B \rightarrow \overline{B}$ should be observed as the preferred interconversion in the two-ring flip mechanism.[12] Consequently, the threshold rotation mechanism for **4** is determined by a comparison with the activation energies between the interconversion of $A \rightarrow \overline{B}$ (or $\overline{A} \rightarrow B$) and that of $B \rightarrow \overline{B}$.

Simulations of the temperature-dependent ^{1}H NMR spectra of **4** were achieved similarly to those of **1b**[12,13] using the program DNMR5;[15] the results are also shown in Fig. 1. In contrast to **1b**, the experimental spectra were well consistent with the calculated spectra by a consideration of both $A \rightarrow \overline{B}$ (and $\overline{A} \rightarrow B$) and $B \rightarrow \overline{B}$ interconversions.

The energy relationships among the stereoisomers and the magnitudes of the barriers separating these isomers were calculated from the data of the simulation over the range from 30 to 120 °C. The results are shown schematically in Fig. 4. The relative intensities of the signals at 30 °C indicate that $B\overline{B}$ is slightly more stable than $A\overline{A}$ at that temperature. A calculation (PM3)[16] of the heat-of-formation of A and B agrees with the relative stabilities of these stereoisomers (Fig. 2). When the sample is warmed, the population of $B\overline{B}$ increases relative to that of $A\overline{A}$. Qualitatively, this indicates a positive entropy difference for the equilibrium ($A\overline{A} \rightarrow B\overline{B}$). $\Delta H°$ (4.1±0.3 kJ mol^{-1}), $\Delta S°$ (20±0.9 J K^{-1} mol^{-1}), and $\Delta G°_{20}$ (−1.7±0.4 kJ mol^{-1}) were calculated from the population data of $A\overline{A}$ and $B\overline{B}$ over the 30—120 °C range. The crossover temperature is therefore ca. −66 °C.

The calculation of the rate data yielded the barriers for the conversion of $A\overline{A}$ to $B\overline{B}$ ($\Delta G^{\neq}_{20}$=78.0 ± 2.1 kJ mol^{-1}) and for the enantiomerization of B and $\overline{B}$ ($\Delta G^{\neq}_{20}$=73.4 ± 2.1 kJ mol^{-1}). Therefore, for the reverse reaction ($B\overline{B} \rightarrow A\overline{A}$), $\Delta G^{\neq}_{20}$=79.7±2.1 kJ mol^{-1}. The lower activation energy of the process $B \rightarrow \overline{B}$ than that of $B \rightarrow \overline{A}$ and ($\overline{B} \rightarrow A$) indicates that the threshold rotation mechanism for **4** is a two-ring flip, in contrast to a one-ring flip for **1b**. These activation energies ($\Delta G^{\neq}_{20}$) were higher than those for **1b** due to increased crowding in the transition state for rotation. This fact provides support strong for our postulate[12] that the two-ring flip defines the high-energy pathways for tri(1-azulenyl)methyl cations.

Dynamic Stereochemistry of the Methane (5). The dynamic stereochemistry of the methane derivative (**5**) was studied and compared with that of the carbocation (**4**). The ^{1}H NMR (600 MHz, methyl region) spectra of **5** in 50% CD_2Cl_2/CS_2 at various temperatures are shown in Fig. 5. At −100 °C, the NMR of **5** consisted of four methyl signals (as indicated by a, b, c, and d in Fig. 5), having a ratio of the intensities of ca. 1 : 1 : 1 : 3.4. Increasing the temperature to ca. −40 °C began to produce noticeable line broadening; further

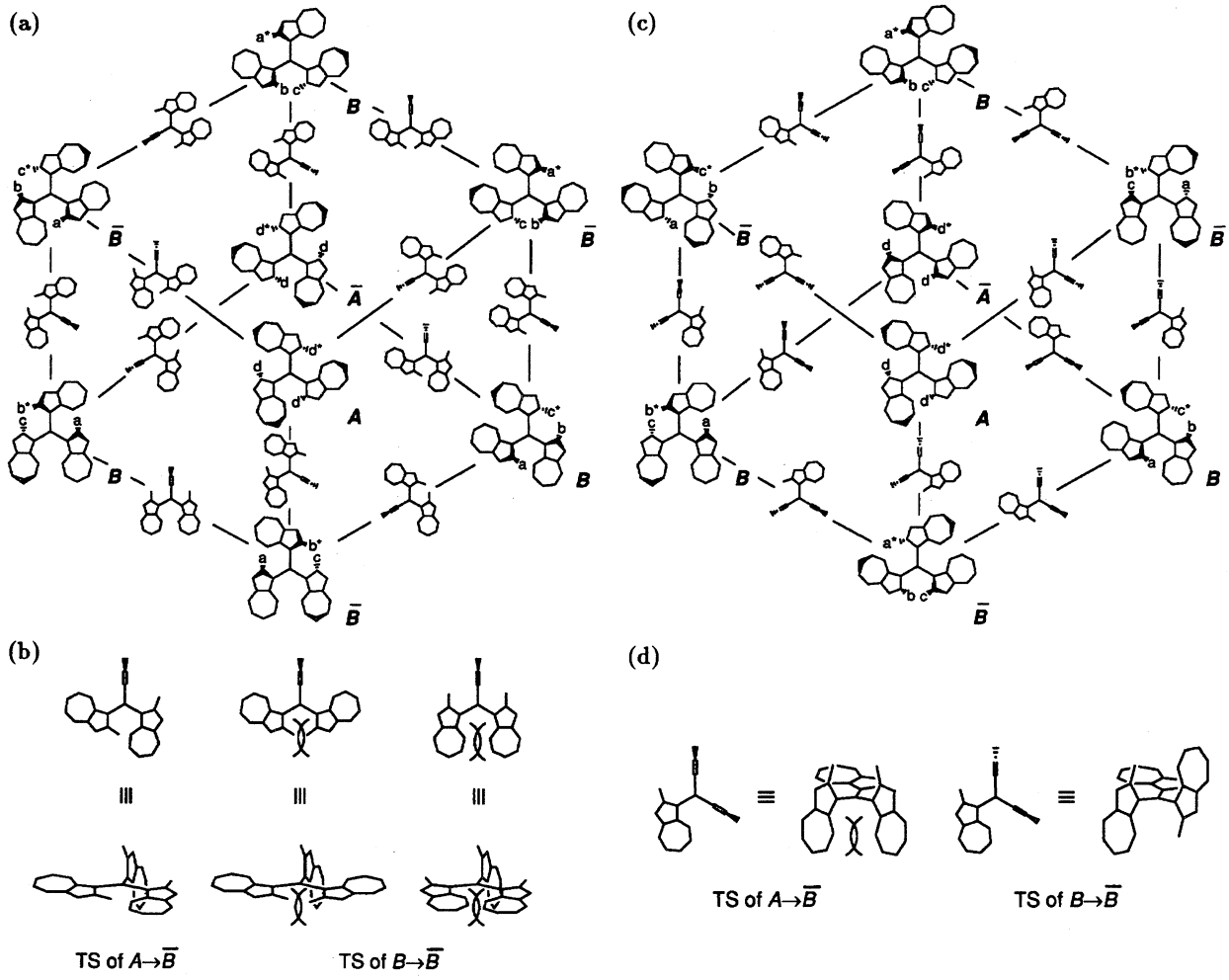

Fig. 3. Possible interconversion of the stereoisomers ($A\overline{A}$ and $B\overline{B}$) and the idealized transition state (TS) for **4**. (a) One-ring flip mechanism for **4**; (b) TS of the one-ring flip for **4**; (c) Two-ring flip mechanism for **4**; (d) TS of the two-ring flip for **4**. The asterisks indicate the three magnetically distinguishable positions during the course of the interconversions.

warming of the sample resulted in the coalescence of all four peaks to a singlet, which became sharp at 40 °C. These spectra indicate that the ground state of **5** is a propeller (helical) conformation. Therefore, the possibilities for the stereoisomerism of **5** should be analyzed by the flip mechanism.[2—4)]

In constant to **4** and **1b** with a trigonal central atom, the propeller blades (azulene rings) of **5** are attached to a tetrahedral carbon, which adapts a pyramidal configuration. Therefore, eight isomeric propeller conformations ($A_1\overline{A_1}$, $A_2\overline{A_2}$, $B_1\overline{B_1}$, and $B_2\overline{B_2}$) are possible for a molecule of this type (**5**), as illustrated in Fig. 6. They were characterized by the torsion angles, which were defined by Φ_i=H–C–C(j1)–C(j2). A_1 (Φ,Φ,Φ) and $\overline{A_1}$ $(-\Phi,-\Phi,-\Phi)$ have C_3 symmetries, and each enantiomer has three equivalent methyl groups. A_2 $(\Phi+\pi,\Phi+\pi,\Phi+\pi)$ and $\overline{A_2}$ $(-\Phi-\pi,-\Phi-\pi,-\Phi-\pi)$ also take C_3 symmetries, and the three methyl groups of each enantiomer are also equivalent. $B_1\overline{B_1}$ $((\Phi,\Phi+\pi,\Phi),(-\Phi,-\Phi-\pi,-\Phi))$ and $B_2\overline{B_2}$ $((\Phi+\pi,\Phi+\pi,\Phi),(-\Phi-\pi,-\Phi-\pi,-\Phi))$ adapt C_1 symmetries; each stereoisomer has three nonequivalent methyl groups. Therefore, the four methyl signals (a, b, c, and d) in the low-temperature ^{1}H NMR spectra show that compound (**5**) exists in one set of four possible combinations: either $A_1\overline{A_1}$ or $A_2\overline{A_2}$ and $B_1\overline{B_1}$ or $B_2\overline{B_2}$. Consequently, the spectrum of **5** at −100 °C was considered to show that the ground state conformation of **5** is a propeller geometry, and that the ratio of $A_1\overline{A_1}$ or $A_2\overline{A_2}$ to $B_1\overline{B_1}$ or $B_2\overline{B_2}$ is ca. 3.4 : 3.0.

The zero-ring flip processes of **5** ($A_1\rightarrow\overline{A_2}$ (site exchange of $d_1\rightarrow d_2$) and $B_1\rightarrow\overline{B_2}$ (site exchange of $a_1\rightarrow a_2$, $b_1\rightarrow b_2$, and $c_1\rightarrow c_2$)) can not explain the temperature dependence of the ^{1}H NMR spectra of **5**, which is similar to that of **4**. The three-ring flip processes of **5** ($A_1\rightarrow\overline{A_1}$ (no site exchange), $A_2\rightarrow\overline{A_2}$ (no site exchange), $B_1\rightarrow\overline{B_1}$ (site exchange of $a_1\rightarrow b_1$), and $B_2\rightarrow\overline{B_2}$ (site exchange of $a_2\rightarrow b_2$)) also can not explain the temperature dependence of the ^{1}H NMR spectra. Furthermore, the transition states of the one- (all three azulene rings rotate through the reference plane) and three-ring flip processes (all the three rings rotate through planes perpen-

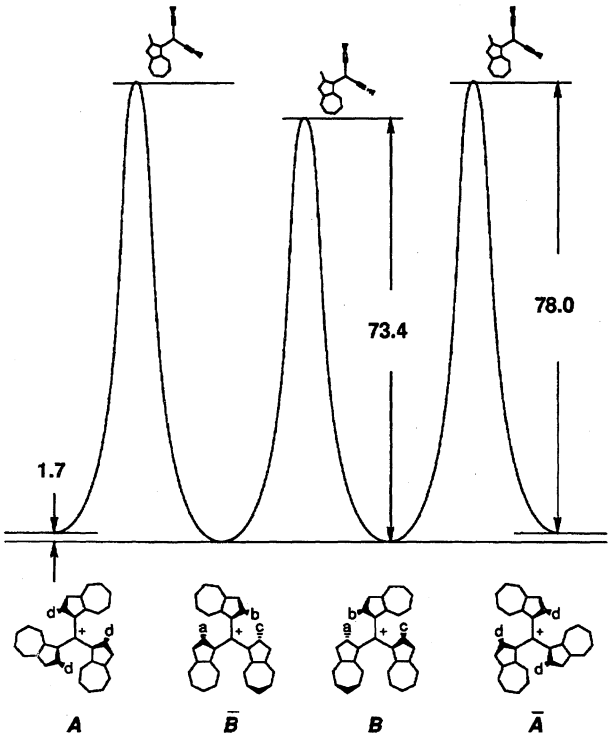

Fig. 4. Schematic representation of the energetics (ΔG/kJ mol^{-1} at 20 °C) of stereoisomerization of **4**.

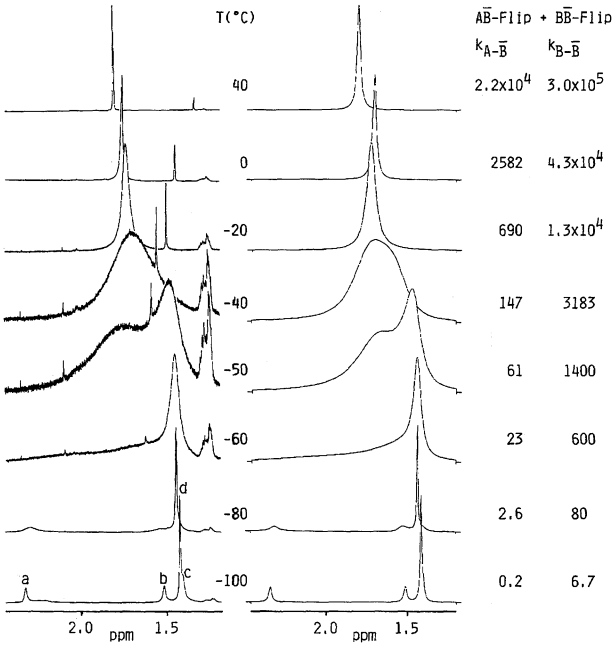

Fig. 5. ^{1}H NMR of **5** (600 MHz, methyl region) at various temperatures. The left-hand panel displays the experimental spectra. The right-hand panel shows the calculated spectra for the combination of the type $A\rightarrow\overline{B}$ (or $\overline{A}\rightarrow B$) and $B\rightarrow\overline{B}$ flip.

dicular to the reference plane) are unfavorable on steric grounds.[12,13] Therefore, those mechanisms are excluded from an analysis of the dynamic behavior of **5**. The residual one- and two-ring flip mechanisms and the ide-

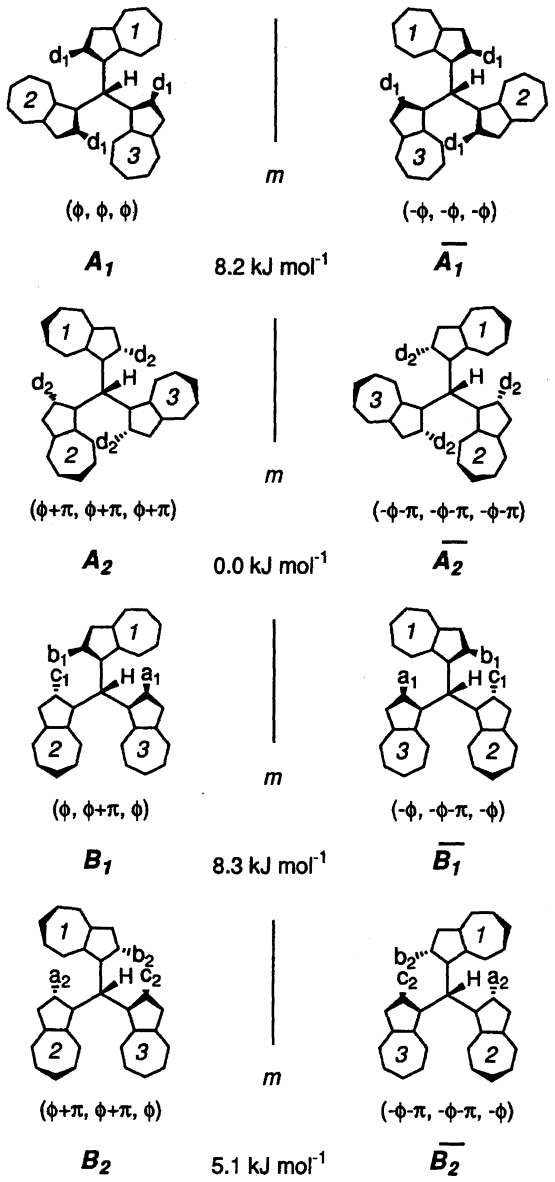

Fig. 6. Stereoisomers of **5**, which were characterized by the torsion angles, and calculated (PM3) relative heat of formation for those of **5**. The methyl groups of the stereoisomers ($A_1\overline{A_1}$, $A_2\overline{A_2}$, $B_1\overline{B_1}$, and $B_2\overline{B_2}$) are labeled by letters a_1—d_1 and a_2—d_2.

alized transition states of the two mechanisms for the stereoisomerization of **4** are illustrated in Fig. 7. There is a total of ten distinct pathways in the two flip mechanisms (six in the one-ring flip and four in the two-ring flip). Those are classified into two types: one is an interconversion of the unsymmetrical propellers, type $B\rightarrow\overline{B}$ ($B_1\rightarrow\overline{B_1}$ or $B_2\rightarrow\overline{B_2}$); the other is those between the symmetrical propellers and unsymmetrical propellers, type $A\rightarrow\overline{B}$ ($A_1\rightarrow\overline{B_1}$ or $A_2\rightarrow\overline{B_2}$).

In the one-ring flip (Fig. 7a), the anti-parallel arrangement of the nonflipping two azulene rings (transition states of the type $A\rightarrow\overline{B}$ (and the type $\overline{A}\rightarrow B$)) is considered to reduce the steric interaction, compared with the

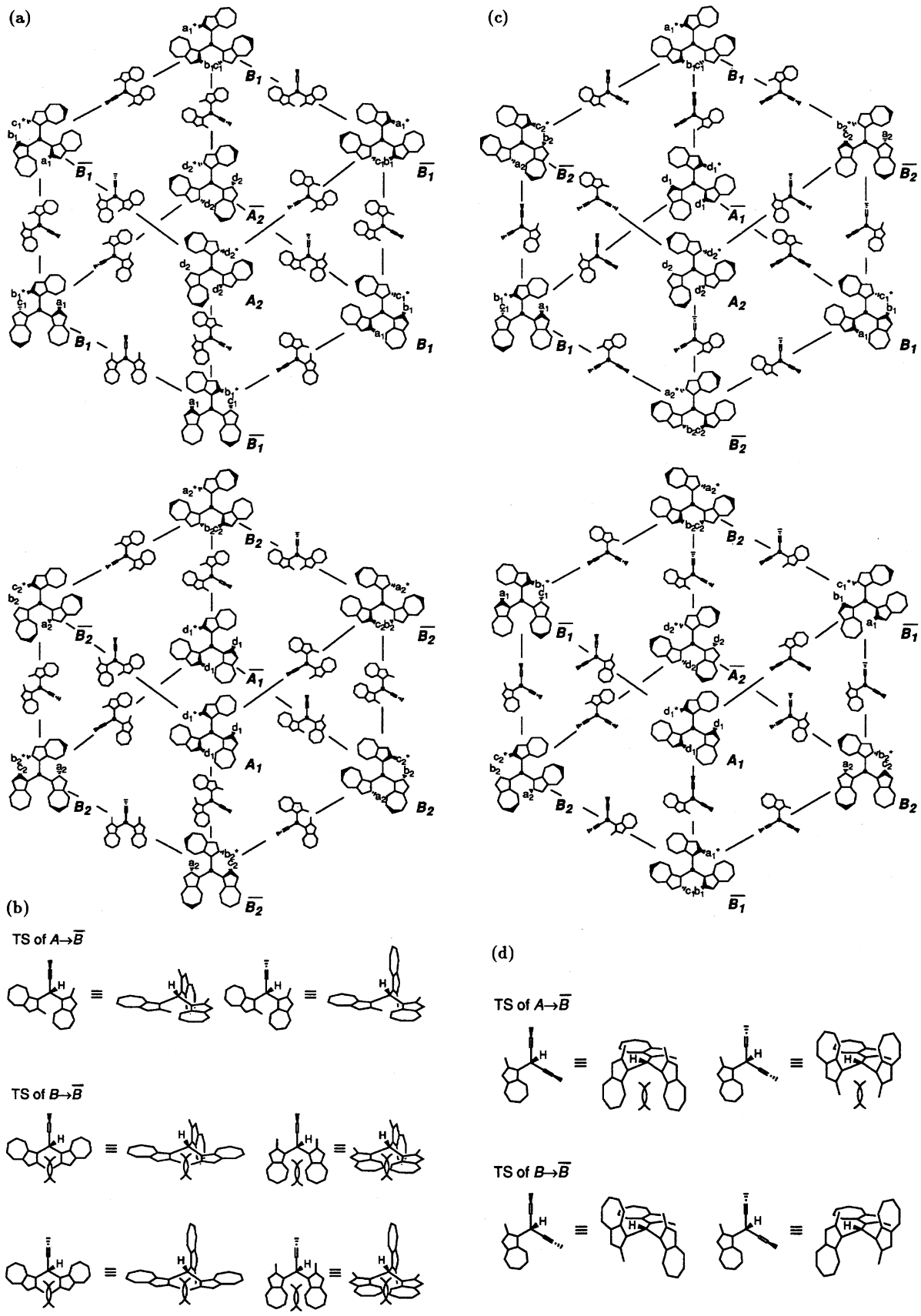

Fig. 7. Possible interconversion of the stereoisomers ($A_1\overline{A_1}$, $A_2\overline{A_2}$, $B_1\overline{B_1}$, and $B_2\overline{B_2}$) and indealized transition state (TS) for **5**. (a) One-ring flip mechanism for **5**; (b) TS of the one-ring flip for **5**; (c) Two-ring flip mechanism for **5**; (d) TS of the two-ring flip for **5**. The asterisks indicate six magnetically distinguishable positions during the course of the interconversions.

parallel arrangement (those of the type $B \rightarrow \overline{B}$) (Fig. 7b), because the four transition states of the interconversions of the type $B \rightarrow \overline{B}$ entail the placement of the 7- and 8-positions and the 2-methyl groups of the nonflipping two azulene rings in essentially the same location, respectively (Fig. 7b). Therefore, the three exchanges (a→d, b→d, and c→d) of the methyl groups by the type $A \rightarrow \overline{B}$ (and the type $\overline{A} \rightarrow B$) should be observed as preferred interconversions in the one-ring flip mechanism.[12]

In the two-ring flip (Fig. 7c), the anti-parallel arrangement of the flipping two azulene rings (transition state of the type $B \rightarrow \overline{B}$) is considered to reduce the steric interaction, compared with the parallel arrangement (that of the type $A \rightarrow \overline{B}$), because the transition state of the interconversion of the type $A \rightarrow \overline{B}$ entails the placement of 8-positions of the flipping two azulene rings in essentially the same location (Fig. 7d). Therefore, the three exchanges (a→b, a→c, and b→c) of the methyl groups by $B \rightarrow \overline{B}$ should be observed as preferred interconversion in the two-ring flip mechanism.[12] Consequently, the threshold rotation mechanism for **5** is also determined by comparisons of the activation energies ($\Delta G^{\neq}$) between the interconversion of the type $A \rightarrow \overline{B}$ (or the type $\overline{A} \rightarrow B$) and those of the type $B \rightarrow \overline{B}$.

Simulations of the variable temperature ^{1}H NMR spectra of **5** were achieved iteratively using the program DNMR5[15] by employing the three energetically equal exchanges (a→b, a→c, and b→c) of the methyl groups by the interconversion of the type $B \rightarrow \overline{B}$ and the three energetically equal exchanges (a→d, b→d, and c→d) of the methyl groups by the interconversion of the type $A \rightarrow \overline{B}$ (or $\overline{A} \rightarrow B$). The results are also shown in Fig. 5. The energy relationships among the stereoisomers of **5** and the magnitudes of the barriers separating these isomers (type $A\overline{A}$ and $B\overline{B}$) were calculated from the spectral data. The relative intensities of the NMR signals at −100 °C show that type $B\overline{B}$ is slightly more stable than type $A\overline{A}$ at this temperature. As the sample is warmed, the population of type $B\overline{B}$ increases relative to that of type $A\overline{A}$. A plot of ΔG° over the range from −100 to −80 °C yields $\Delta H°$=4.1±1.0 kJ mol^{-1} and $\Delta S°$=23±5.7 J K^{-1} mol^{-1} for the equilibrium of type $A\overline{A}$→type $B\overline{B}$. Therefore, the crossover temperature is ca. −93 °C.

The rate data determined by an iterative analysis of the temperature-dependent ^{1}H NMR spectra of **5** were used to calculate the free energies of activation for the various exchange processes at 20 °C. The results are shown schematically in Fig. 8. For the equilibrium of type $A\overline{A}$→type $B\overline{B}$, $\Delta G°_{20}$ is −2.6±1.9 kJ mol^{-1}. For the conversion of type $A\overline{A}$ to type $B\overline{B}$, the calculations yielded $\Delta G^{\neq}_{20}$=49.9±2.0 kJ mol^{-1}; for the reverse reaction (type $B\overline{B}$→type $A\overline{A}$), $\Delta G^{\neq}_{20}$=52.5±2.8 kJ mol^{-1}. The barrier to the isomerization of type $B\overline{B}$ is $\Delta G^{\neq}_{20}$=43.2±1.7 kJ mol^{-1}. Thus, the isomerization of type $B\overline{B}$ to type $B\overline{B}$ is energetically more favorable by 9.3 kJ mol^{-1} than that of type $B\overline{B}$ to type $A\overline{A}$ at

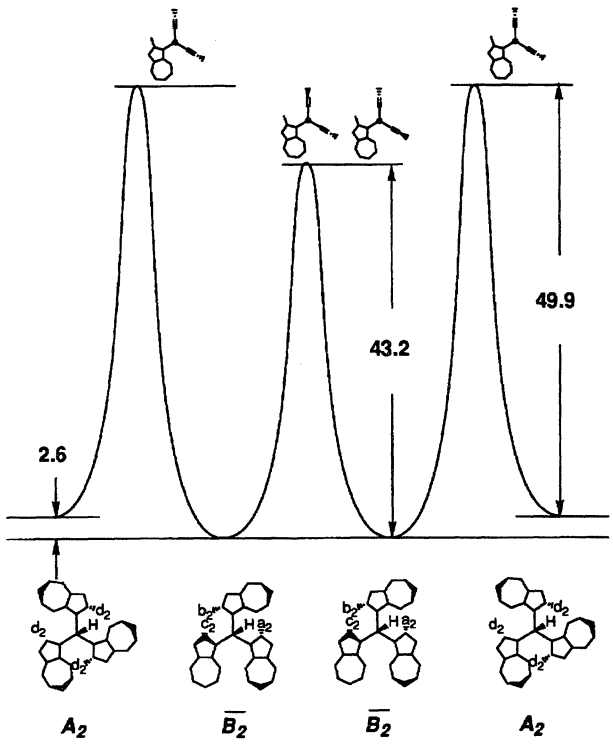

Fig. 8. Schemetic representation of the energetics (ΔG/kJ mol^{-1} at 20 °C) of stereoisomerization of **5**.

20 °C. The lower activation energy of type $B \rightarrow \overline{B}$ than that of type $B \rightarrow \overline{A}$ (and the type $\overline{B} \rightarrow A$) indicates that the threshold rotation mechanism for **5** is a two-ring flip in contrast to a one-ring flip for **1b**.

Considerations of the stabilities of the conformers ($A_1\overline{A_1}$, $A_2\overline{A_2}$, $B_1\overline{B_1}$, and $B_2\overline{B_2}$) using the molecular models and the calculated (PM3)[16] heat of formation, as shown in Fig. 6, of the stereoisomers (A_1,A_2,B_1, and B_2), demonstrate that $A_2\overline{A_2}$ and $B_2\overline{B_2}$ are more stable stereoisomers than $A_1\overline{A_1}$ and $B_1\overline{B_1}$. Therefore, the four observed resonances (a, b, c, and d) of **5** are considered as being $B_2\overline{B_2}$ (a_2, b_2, and c_2) and $A_2\overline{A_2}$ (d_2). The threshold mechanism for **5** was also consistent with this assignment of the methyl groups of **5**. Although the two-ring flip for **5** interconverts A_2 to $\overline{B_2}$ (and $\overline{A_2}$ to B_2), the one-ring flip for **5** does not interconvert A_2 to $\overline{B_2}$ (and $\overline{A_2}$ to B_2). Therefore, the observed coalescence of **5** in the temperature-dependent ^{1}H NMR spectra is a result of the interconversion of $B_2 \rightarrow \overline{B_2}$ in a two-ring flip and the combination with those of $A_2 \rightarrow \overline{B_2}$ (and $A_2 \rightarrow \overline{B_2}$) in a two-ring flip.

The Comparison of the Activation Energies. The activation energies ($\Delta G^{\neq}_{20}$ and $\Delta G°_{20}$/kJ mol^{-1}) for the stereoisomerization of **1b**,[12,13] **4**, and **5** are summarized in Table 4. The $\Delta G°_{20}$ ($A\overline{A} \rightarrow B\overline{B}$) values of **1b**, **4**, and **5** are approximately equal to each other (−1.7—−3.2 kJ mol^{-1}). The values indicate that the unsymmetrical propeller conformations (type $B\overline{B}$) are slightly more stable than the symmetrical propeller conformations (type $A\overline{A}$).

Table 4. The $\Delta G^{\neq}_{20}$ and the ΔG°_{20} Values (kJ mol^{-1} at 20 °C) for the Stereoisomerization of **1b**,[12,13] **4**, and **5**

	Threshold rotation mechanism	$\Delta G^{\neq}_{20}$ ($A\overline{A}\rightarrow B\overline{B}$)	$\Delta G^{\neq}_{20}$ ($B\overline{B}\rightarrow B\overline{B}$)	ΔG°_{20} ($A\overline{A}\rightarrow B\overline{B}$)
1b	One-ring flip	55.5±5.1	61.8±5.1	−3.3±0.5
4	Two-ring flip	78.0±2.1	73.4±2.1	−1.7±0.4
5	Two-ring flip	49.9±2.0	43.2±1.7	−2.6±1.9

The 2-methyl groups on the azulene should restrict ring flipping to a considerable extent, because the steric interactions among the three azulene rings of **4** and **5** are larger than those of **1b**. Therefore, the larger $\Delta G^{\neq}$ values of both $A\rightarrow\overline{B}$ and $B\rightarrow\overline{B}$ flip of **1b** compared to those of **5** are attributed to the large conjugative interaction between the central cation and the three azulene rings, which changes the threshold rotation mechanism for **1b** to a one-ring flip. The $\Delta G^{\neq}$ values of both the $A\rightarrow\overline{B}$ and $B\rightarrow\overline{B}$ flip of **4** are much larger than those of **1b**. The large $\Delta G^{\neq}$ values of **4** arise from a steric interaction among the three 2-methyl groups, which reverted the threshold mechanism of **4** to a two-ring flip.

Conclusion. The dynamic stereochemistry of **4** showed that the threshold rotation mechanism for the tri(1-azulenyl)methyl cations is not uniformly a one-ring flip, but is variable due to the contribution of the steric effect of the three azulene rings. A comparison of the dynamic stereochemistry of the methane derivative (**5**) with those of **1b** and **4** indicate that the conjugative effect between the cationic carbon and the three azulene rings largely contribute to the transition state of the ring flipping as well as to the ground state.

Experimental

General. The melting points were determined on a Yanagimoto micro melting-point apparatus (MP-S3), and are uncorrected. The electron-impact mass spectra were obtained using a JEOL HX-110 instrument, usually at 70 eV. IR and UV spectra were measured on a Hitachi 270-30 and a Hitachi U-3410 spectrophotometer, respectively. ^{1}H NMR spectra were recorded on a Hitachi R-90H at 90 MHz or a Bruker AM 600 spectrometer at 600 MHz. ^{13}C NMR spectra were recorded on a Hitachi R-90H at 22.5 MHz or a Bruker AM 600 spectrometer at 150 MHz. Gel-permeation chromatographies (GPC) were performed on Showadenko Shodex K2001 and K2002. Voltammetry measurements were carried out with a BAS100B/W electrochemical workstation equipped with Pt working and auxiliary electrodes, and a reference electrode formed from Ag/$AgNO_3$ (0.01 M, 1 M=1 mol dm^{-3}) and tetrabutylammonium perchlorate solution (0.1 M) in MeCN. All of the measurements were made under argon on a 1 mM sample of the substrate in 10 ml of dry MeCN containing 0.1 M tetraethylammonium perchlorate (TEAP) as a supporting electrolyte at a scan rate of 100 mV s^{-1}. Elemental analyses were performed at the Instrumental Analysis Center of Chemistry, Faculty of Science, Tohoku University.

Tris(2-methyl-1-azulenyl)methane (5). A solution of 2-methylazulene (**6**) (260 mg, 1.83 mmol) and 1-formyl-2-methylazulene (**7**) (156 mg, 0.92 mmol) in glacial acetic acid (1.7 ml) and CH_2Cl_2 (1.7 ml) was pressed at 10 kbar at 30 °C for 24 h. The reaction mixture was poured into water, alkalified with 5% aqueous $NaHCO_3$, and extracted with CH_2Cl_2. The organic layer was washed with water, dried with $MgSO_4$, and concentrated in vacuo. The residue was purified by column chromatography on silica gel with CH_2Cl_2 and GPC with $CHCl_3$ to afford the tri(1-azulenyl)methane (**5**) (142 mg, 49%) and 1,3-bis[bis(2-methyl-1-azulenyl)methyl]-2-methylazulene (**8**) (15 mg, 5%).

5: Blue plates; mp 267.5—273.0 °C (CH_2Cl_2/hexane); MS (70 eV) m/z (rel intensity) 436 (M^+; 100), 421 (45), 279 (39), and 278 (26); IR (KBr disk) 1570, 1488, and 1408 cm^{-1}; UV (CH_2Cl_2) 241 (log ε 4.65), 286 (5.01), 358 (4.10), 375 (3.91), and 590 nm (2.87); ^{1}H NMR (600 MHz, 50% CD_2Cl_2/CS_2) δ=8.079 (d, J=9.5 Hz, 3H), 7.606 (d, J=9.9 Hz, 3H), 7.426 (s, 1H), 7.306 (dd, J=9.8, 9.8 Hz, 3H), 7.082 (s, 3H), 6.985 (dd, J=9.8, 9.5 Hz, 3H), 6.676 (dd, J=9.8, 9.8 Hz, 3H), and 1.790 (s, 9H). Found: m/z 436.2194. Calcd for $C_{34}H_{28}$: M, 436.2191. Found: C, 93.06; H, 6.71%. Calcd for $C_{34}H_{28}$: C, 93.54; H, 6.46%.

8: Blue crystals; mp 176.0—185.0 °C decomp (CH_2Cl_2/hexane); MS (70 eV) m/z (rel intensity) 730 (M^+; 5), 292 (24), 142 (100), 141 (82), and 115 (25); IR (KBr disk) 1572, 1410, and 740 cm^{-1}; UV (CH_2Cl_2) 242 (log ε 4.84), 285 (5.17), 357 (4.27), and 594 nm (3.07); ^{1}H NMR (600 MHz, 50% CD_2Cl_2/CS_2) δ=8.062 (d, J=9.4 Hz, 1H, $H_{4'}$), 8.051 (d, J=9.4 Hz, 3H, $H_{4'}$), 7.622 (d, J=9.8 Hz, 2H, $H_{4,8}$), 7.587 (d, J=9.8 Hz, 1H, $H_{8'}$), 7.575 (d, J=9.8 Hz, 1H, $H_{8'}$), 7.560 (d, J=9.8 Hz, 1H, $H_{8'}$), 7.553 (d, J=9.8 Hz, 1H, $H_{8'}$), 7.380 (s, 1H, CH), 7.365 (s, 1H, CH), 7.300 (dd, J=9.7, 9.6 Hz, 1H, $H_{6'}$), 7.294 (dd, J=9.7, 9.6 Hz, 3H, $H_{6'}$), 7.140 (t, J=9.8 Hz, 1H, H_6), 7.062 (s, 3H, $H_{3'}$), 7.052 (s, 1H, $H_{3'}$), 6.969 (dd, J=9.6, 9.4 Hz, 1H, $H_{5'}$), 6.964 (dd, J=9.6, 9.4 Hz, 3H, $H_{5'}$), 6.622 (dd, J=9.8, 9.7 Hz, 1H, $H_{7'}$), 6.606 (dd, J=9.8, 9.7 Hz, 1H, $H_{7'}$), 6.603 (dd, J=9.8, 9.7 Hz, $H_{7'}$), 6.590 (dd, J=9.8, 9.7 Hz, 1H, $H_{7'}$), 6.535 (dd, J=9.8, 9.8 Hz, 2H, $H_{5,7}$), 1.855 (s, 3H, 2′-Me), 1.843 (s, 3H, 2′-Me), 1.830 (s, 3H, 2′-Me), 1.825 (s, 3H, 2′-Me), and 1.394 (s, 3H, 2-Me); ^{13}C NMR (150 MHz, 50% CD_2Cl_2/CS_2) δ=151.253 (s, C_2), 151.104 (s, $C_{2'}$), 151.085 (s, 2C, $C_{2'}$), 151.072 (s, $C_{2'}$), 140.813 (s, $C_{3'a}$), 140.791 (s, $C_{3'a}$), 140.763 (s, 2C, $C_{3'a}$), 137.171 (s, 3C, $C_{8'a}$), 137.151 (s, $C_{8'a}$), 137.030 (s, $C_{3a,8a}$), 136.549 (d, C_6), 136.340 (d, $C_{6'}$), 136.322 (d, 3C, $C_{6'}$), 134.781 (d, 4C, $C_{4'}$), 132.976 (d, $C_{8'}$), 132.940 (d, 3C, $C_{8'}$), 132.763 (d, $C_{4,8}$), 129.922 (s, $C_{1'}$), 129.881 (s, 3C, $C_{1'}$), 129.503 (s, C_1 or C_3), 129.487 (C_1 or C_3), 123.522 (d, 4C, $C_{5'}$), 122.899 (d, 3C, $C_{7'}$), 122.882 (d, $C_{7'}$), 122.730 (d, $C_{5,7}$), 120.081 (d, $C_{3'}$), 120.070 (d, $C_{3'}$), 120.053 (d, $C_{3'}$), 120.033 (d, $C_{3'}$), 38.032 (d, CH), 37.980 (d, CH), 16.736 (q, 2′-Me), 16.671 (q, 3C, 2′-Me), and 14.068 (q, 2-Me). Found: m/z 784.5060. Calcd for $C_{57}H_{46}$: M, 784.5008. Found: C,

93.43; H, 6.49%. Calcd for $C_{57}H_{46}$: C, 93.66; H, 6.34%.

Tris(2-methyl-1-azulenyl)methyl Hexafluorophosphate (4·PF_6^-). DDQ (32 mg, 0.14 mmol) was added at room temperature to a solution of tris(2-methyl-1-azulenyl)methane (**5**) (42 mg, 0.096 mmol) in CH_2Cl_2 (40 ml). The blue solution turned deep blue. After the solution was stirred at the same temperature for 1 h, concentrated HPF_6 (2 ml) was slowly added. After stirring at room temperature for an additional 15 min, water (20 ml) was added to the mixure. After the resulting suspension was filtered with suction, the organic layer was separated, washed with water, dried with $MgSO_4$, and concentrated under reduced pressure. After the residue was dissolved in CH_2Cl_2 (1 ml), Et_2O (30 ml) was added to the solution. The precipitated crystals was filtered off, washed with Et_2O, and dried in vacuo to give the tri(1-azulenyl)methyl hexafluorophosphate (4·PF_6^-) (56 mg, 100%). Deep purple powder; mp>300 °C (CH_2Cl_2/ether); MS (FAB) *m/z* 435 (M^+-PF_6); IR (KBr disk) 1429, 1408, 1278, 840, and 558 cm^{-1}; UV (CH_2Cl_2) 231 (log ε 4.75), 256 (4.68), 295 (4.61), 332 (4.36), 416 (3.93), 624 (4.70), and 649 nm (4.69); ^{1}H NMR (600 MHz, DMSO-d_6) δ=8.717 (d, *J*=9.7 Hz, 3H), 8.708 (d, *J*=9.5 Hz, 1H), 8.692 (d, *J*=9.3 Hz, 1H), 8.684 (d, *J*=9.5 Hz, 1H), 7.988 (dd, *J*=9.8, 9.7 Hz, 3H), 7.929 (dd, *J*=9.8, 9.7 Hz, 1H), 7.874 (dd, *J*=9.7, 9.7 Hz, 4H), 7.831 (dd, *J*=9.7, 9.5 Hz, 1H), 7.821 (dd, *J*=9.8, 9.7 Hz, 1H), 7.804 (dd, *J*=9.7, 9.3 Hz, 1H), 7.795 (d, *J*=9.9 Hz, 3H), 7.768 (dd, *J*=9.7, 9.5 Hz, 1H), 7.752 (s, 1H), 7.683 (s, 1H), 7.674 (s, 1H), 7.637 (d, *J*=9.9 Hz, 1H), 7.609 (s, 3H), 7.555 (d, *J*=9.9 Hz, 1H), 7.512 (dd, *J*=9.9, 9.8 Hz, 3H), 7.434 (dd, *J*=9.9, 9.8 Hz, 1H), 7.400 (d, *J*=9.9 Hz, 1H), 7.335 (dd, *J*=9.9, 9.7 Hz, 1H), 7.268 (dd, *J*=9.9, 9.8 Hz, 1H), 2.045 (s, 3H), 1.984 (s, 3H), 1.694 (s, 3H), and 1.629 (s, 9H). Found: *m/z* 435.2071. Calcd for $C_{34}H_{27}^+$: M^+, 435.2113. Found: C, 71.16; H, 4.56%. Calcd for $C_{34}H_{27}PF_6$: C, 70.34; H, 4.69%.

pK_{R+} Value. A sample solution of the cations **4** was prepared by dissolving in a glycine (0.1 M) solution (50 ml), and made up to 100 ml by adding MeCN; and the sample solution with lower acidity was made by further alkalification with 20% aqueous NaOH. The concentration of the cation was determined spectrophotometrically at 24 °C. The pH of each sample was measured on a Horiba pH meter F-13 calibrated with standard buffers before use. The observed absorbance at the specific absorption maxima of the cation (**4**) was plotted against the pH, giving a classical titration curve whose midpoint was taken as the pK_{R+} value.

^{1}H and ^{13}C NMR spectra and the complete spectral data of MS, IR, UV, ^{1}H NMR, and ^{13}C NMR for the reported compounds (**4**, **5**, and **8**) are deposited as Document No. 68043 at the Office of the Editor of Bull. Chem. Soc. Jpn.

The authors gratefully acknowledge Professor Tsutomu Miyashi of this department for his help to running the PM3 calculations on a Tektronix CAChe WorkSystem. This work was supported by a Grant-in-aid for Scientific Research No. 03854053 to S. I. and that on Priority Areas (No. 02230103) to T. A. from the Ministry of Education, Science and Culture, and the Research Aid of Inoue Foundation for Science.

References

1) A part of this work has been published in preliminary form: S. Ito, N, Morita, and T. Asao, *Tetrahedron Lett.*, **35**, 3723 (1994).

2) A. K. Colter, I. I. Schuster, and R. J. Kurkland, *J. Am. Chem. Soc.*, **87**, 2278 (1965).

3) R. J. Kurkland, I. I. Schuster, and A. K. Colter, *J. Am. Chem. Soc.*, **87**, 2279 (1965).

4) I. I. Schuster, A. K. Colter, and R. J. Kurkland, *J. Am. Chem. Soc.*, **90**, 4679 (1968).

5) J. W. Rakshys, Jr., S. V. McKindley, and H. H. Freedman, *J. Am. Chem. Soc.*, **92**, 3518 (1970).

6) J. W. Rakshys, Jr., S. V. McKindley, and H. H. Freedman, *J. Am. Chem. Soc.*, **93**, 6522 (1971).

7) F. Strohbusch, *Tetrahedron*, **28**, 1915 (1972).

8) J. F. Blount, P. Fincchiaro, D. Gust, and K. Mislow, *J. Am. Chem. Soc.*, **95**, 7019 (1973).

9) J. P. Hummel, D. Gust, and K. Mislow, *J. Am. Chem. Soc.*, **96**, 3679 (1974).

10) S. Ito, N. Morita, and T. Asao, *Tetrahedron Lett.*, **32**, 773 (1991).

11) S. Ito, N. Morita, and T. Asao, *Tetrahedron Lett.*, **35**, 751 (1994).

12) S. Ito, N. Morita, and T. Asao, *Bull. Chem. Soc. Jpn.*, **68**, 1409 (1995).

13) S. Ito, N. Morita, and T. Asao, *Tetrahedron Lett.*, **33**, 6669 (1992).

14) S. Ito, N. Morita, and T. Asao, *Bull. Chem. Soc. Jpn.*, **68**, 2011 (1995).

15) D. S. Stephenson and G. Binsch, *QCPE*, **10**, 365 (1978).

16) PM3 semiempirical MO calculations in Figs. 2 and 6 were performed by the MOPAC version 6 on a Tektronix CAChe WorkSystem.